

# More Power Implies Different Work: ATP-Dependent Actomyosin Remodelling

Sami C. Al-Izzi,<sup>1</sup> Darius V. Köster,<sup>2,\*</sup> and Richard G. Morris<sup>1,†</sup>

<sup>1</sup>*School of Physics and EMBL Australia Node in Single Molecule Science,  
School of Medical Sciences, University of New South Wales - Sydney 2052, Australia*

<sup>2</sup>*Centre for Mechanochemical Cell Biology and Division of Biomedical Sciences,  
Warwick Medical School, University of Warwick, Coventry CV4 7AL, United Kingdom*

Since myosin II motors exert forces on actin filaments upon hydrolysis of Adenosine Triphosphate (ATP), the rate at which energy is converted into mechanical work—the power—is directly proportional to the concentration of available ATP. We now argue that changes in power can also alter the *mode* by which mechanical work is carried out by actomyosin. Using a simplified model of myosin II minifilament kinetics, we motivate a novel active hydrodynamic theory that is consistent with the ATP-dependence of (quasi-)steady states of actomyosin, reconstituted *in vitro* on supported lipid bilayers and observed using interferometric scattering and total internal reflection fluorescence microscopy. Specifically, as ATP concentration increases, our analysis suggests that contractility gives way to the increasingly processive motion of myosin II minifilaments along actin filaments, which results in meta-stable vortex- and spiral-like motifs, as opposed to aster-like structures. The broader implication is a coupling between ATP synthesis (via cellular metabolism) and cortical remodelling, potentially re-framing ATP as not only a fuel, but also a regulator.

## I. INTRODUCTION

Active hydrodynamics—the long wavelength description of systems driven by energy input that can be transduced locally to perform work—has made important contributions to the qualitative understanding and conceptualisation of biological systems at a variety of scales, including bacterial suspensions [1–3], tissues [4–7], developing embryos [8–10], cells [11, 12], and subcellular components *e.g.* microtubules [13]. However, a significant obstacle to making such theories more quantitative is the functional form of so-called active coefficients—counterparts to passive Onsager coefficients—which are unconstrained, and can depend arbitrarily on the dynamical degrees-of-freedom in any theory.

In this context, we revisit actomyosin, the canonical meshwork of actin filaments and myosin II motors that is crucial for many cellular functions [14–16]. Actomyosin is a central example of active matter [17], since the hydrolysis of Adenosine Triphosphate (ATP) by myosin II head-groups permits a so-called power-stroke, locally converting chemical energy into mechanical forces [18]. Nevertheless, evidence from several *in vitro* studies suggests that the relationship between the concentration of available ATP and the behaviour of actomyosin is more complex than current hydrodynamic theories recognise, with ATP influencing actin meshwork pattern formation [19], rheology [20], actin filament breaking [21], and myosin II processivity [22].

Alongside total internal reflection fluorescence (TIRF) microscopy, we now use interferometric scattering (iSCAT) microscopy [23, 24]—a label-free approach that relies on the interference between reflected and scattered

light from nano-objects near an interface—to observe reconstituted actomyosin networks over long times without deterioration and inactivation of myosin due to photodamage. In particular, we report recurrent meta-stable actomyosin structures, such as vortex- and spiral-like motifs, at intermediate ATP concentrations, which we contrast with the aster-like patterns formed upon depletion of ATP.

To account for this behaviour, we invoke scaling arguments derived from a simplified statistical model of myosin II minifilament headgroup kinetics and write down an hydrodynamic theory whose active coefficients qualitatively codify the ATP-dependence of actomyosin remodelling. In doing so, we highlight both potential underlying molecular mechanisms and emergent macroscopic behaviours at the collective/material level. In particular, as ATP concentration increases, our results suggest that contractility gives way to the increasingly processive motion of myosin II minifilaments along actin filaments.

In other words, although the rate at which actomyosin performs work—*i.e.*, the *power*—is directly proportional to the concentration of ATP, more power does not exclusively translate into more of the same work, and changes in ATP concentration alter the *mode* by which the meshwork is remodelled.

## II. ASTERS, SPIRALS AND VORTICES REVISITED

We start with actomyosin reconstituted *in vitro* on supported lipid bilayers [13, 27–32]: a system previously shown to readily remodel under the action of ATP, forming asters and contractile foci under a variety of conditions [28, 29]. Specifically, we follow [22] and use iSCAT microscopy to observe the motion of myosin II minifilaments atop a texture of intermediate length F-actin

\* [d.koester@warwick.ac.uk](mailto:d.koester@warwick.ac.uk)

† [r.g.morris@unsw.edu.au](mailto:r.g.morris@unsw.edu.au)

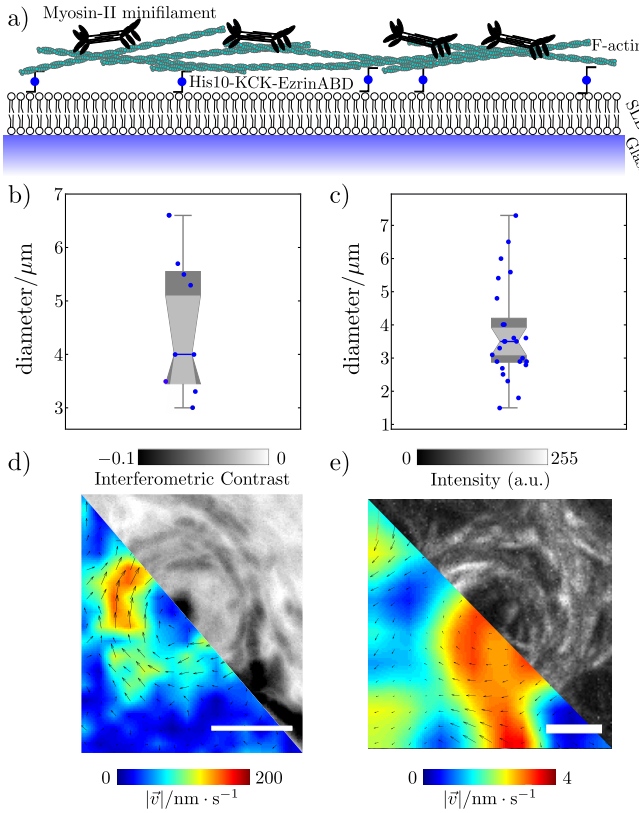


**FIG. 1. Meta-stable vortices and spirals.** **a)** myosin II minifilaments were deposited on a layer of F-actin, itself attached with His10-KCK-EzrinABD to a supported lipid bilayer on a glass substrate (not to scale). **b)** Approximately 10 min after addition of 0.1 mM ATP, networks with intermediate length F-actin ( $l_{\text{actin}} = 8 \pm 4.7 \mu\text{m}$  [25]) and an approximate minifilament-to-actin filament ratio of 3:1 displayed meta-stable spiral-like structures in iSCAT with an average diameter of  $4.5 \pm 1.3 \mu\text{m}$ . **c)** Observing a range of lengths ( $l_{\text{actin}} = 9 \pm 5.5/ 7 \pm 4.7/ 6 \pm 4.6 \mu\text{m}$ ) of fluorescently-labelled actin via TIRF at an approximate minifilament-to-actin ratio of 1:1 resulted in motifs with an average diameter  $3.7 \pm 1.5 \mu\text{m}$ . **d)** Representative minimal intensity projections (duration 120s, scale bar  $2\mu\text{m}$ ) and corresponding flow fields inferred using PIV analysis for iSCAT. **e)** Representative vortex TIRF maximal intensity projection (duration 120s, scale bar  $2\mu\text{m}$ ) with corresponding PIV analysis. (See SM [26] for more details).

( $l_{\text{actin}} = 9 \pm 5.5/ 7 \pm 4.7/ 6 \pm 4.6 \mu\text{m}$ ), itself attached to fluid lipid-bilayer supported by a glass substrate (Fig. 1a). Our central observation is that, whilst aster-like contractile foci can be observed once ATP has been depleted (Vid. 1), at earlier times, when concentrations of ATP are estimated to be around 1-10  $\mu\text{M}$  [19, 21] we also observe complex swirling patterns. These are characterised by recurrent dynamical vortex- and spiral-like motifs, where myosin II minifilaments tightly circle either a void or a myosin II rich centre (Fig. 1d, Vid. 2-5, SM Sec. 2 [26]). On rare occasions, we also see such structures merge to form a larger foci (Vid. 6). The av-

erage diameter of the circular motion was  $4.5 \pm 1.3 \mu\text{m}$ , with particle image velocimetry (PIV) [33–35] characterising peak speeds on the order of  $100 \text{ nm s}^{-1}$  (see SM Sec. 2 [26]). The lifetimes of the motifs all exceeded 90 s, which is far greater than the average residence time of individual minifilaments [22], and indicative of a quasi-stable state whereby the incoming and outgoing fluxes of minifilaments are almost balanced.

Since the iSCAT signal of actin filaments is very low in comparison to the myosin signal, we separately observed fluorescently labelled actin filaments under similar conditions using total internal reflection fluorescence (TIRF) microscopy (Fig. 1c and SM Sec. 1 [26]). Again, this revealed long-lived vortex-like motion (Fig. 1e, Vid. 7–8, SM Sec. 2), with circular motifs of average diameter  $3.7 \pm 1.5 \mu\text{m}$  and lifetimes  $> 100$  s. Strikingly, however, PIV revealed that speeds were  $1 – 5 \text{ nm s}^{-1}$ , significantly slower than those of the myosin II minifilaments (see SM Sec. 2 [26]). Moreover, the actin and myosin vortices flow in the same direction, and almost all the vortices are of the same handedness (29 out of 34). This latter feature we attribute to the chirality of actin inducing a twist-bend coupling [36–38], although a detailed investigation is considered out of scope for this article.

Nominally, such observations bare superficial similarities to the steady-state *asters*, *spirals* and *vortices* reported in a generic treatment of incompressible active polar gels [39]. However, the underlying physics of [39] differs considerably from that of our system, where myosin features explicitly, layered atop actin, and where both actin and myosin are compressible and permit mass transport. (The stratification of myosin and actin has been suggested to be an important organising factor elsewhere [40]). Moreover, there is a lack of evidence for either *i*) a non-negligible passive elastic splay modulus at the densities of actin in our assays, or *ii*) any noticeable active spontaneous-splay stresses that drive the rotation of spirals in [39]. As a result, the only true steady-states in our system should, in principle, be aster-like, which is in-line with the actin textures that we observe on depletion of ATP (and their behaviour on ATP add-back). In order to explain the aforementioned meta-stable structures at higher levels of ATP, we therefore invoke a simple model of myosin II minifilament kinetics to argue that active coefficients in bulk hydrodynamic descriptions of actomyosin must scale non-trivially with the concentration of available ATP.

### III. ACTIVE HYDRODYNAMICS OF *IN VITRO* ACTOMYOSIN

In order to explore the phenomenology that underpins these observations, we write down a nemato-hydrodynamic description of our *in vitro* system (SM Sec. 4 [26] & [17, 39, 41–44]). Whilst this overlooks some non-trivial aspects of the rheology of transiently-bound intermediate-length actin filaments (discussed later) we

argue that such a symmetry-based approach is sufficient if we restrict ourselves to long-lived steady-state and quasi-steady-state behaviours only.

Since the depletion of bulk ATP is slow compared to characteristic myosin II minifilament residence times, we adopt a quasi-static approach to ATP concentration. In this context, using myosin II minifilament residence time and run length as characteristic spatio-temporal scales, there are only two continuity equations, one for the density of myosin II minifilaments

$$\partial_t \rho_m + \nabla \cdot (\vec{v}_m \rho_m) = k - e^{\rho_m}, \quad (1)$$

and one for the density of actin filaments

$$\partial_t \rho_a + \nabla \cdot (\vec{v}_a \rho_a) = 0. \quad (2)$$

---


$$\Sigma = \left( -\zeta + \bar{\nu} \vec{P} \cdot \vec{h} \right) \mathbb{I} + \nu \left[ \vec{P} \vec{h} \right]^S + \left[ \vec{P} \vec{h} \right]^A + (\chi_m \rho_m - \chi_a \rho_a) \mathbb{I} + 2 \eta \left( [\nabla \vec{v}_a]^S - \nabla \cdot \vec{v}_a \mathbb{I} \right) + \bar{\eta} \nabla \cdot \vec{v}_a \mathbb{I}. \quad (5)$$


---

Sans-serif superscripts S and A denote the symmetric and antisymmetric parts, respectively, whilst  $\zeta$  is the active isotropic contractility. The constants  $\nu$  and  $\bar{\nu}$  are the spin connection coefficients,  $\chi_a$  is the dimensionless compressibility for actin, and  $\eta$  and  $\bar{\eta}$  are the shear and bulk viscosities, respectively. The quantity  $\vec{h} = -\delta \mathcal{F} / \delta \vec{P}$ , is the so-called molecular field, which is derived from the elastic free energy of the polarisation field. Ostensibly, the low densities involved in our experiments imply that  $\mathcal{F}$  can be neglected. However, intermediate length actin filaments have a persistence length that is a non-vanishing fraction of their length, permitting bending at relatively low energetic cost [38]. We approximate this behaviour by a standard term that associates a free-energy cost to bending of the polarisation field:

$$\mathcal{F} = \int \frac{\kappa}{2} |\vec{P} \cdot \nabla \vec{P}|^2 dA, \quad (6)$$

where  $\kappa$ — the bend elastic modulus [45]— is small. The system of equations is then closed by the dynamics of the polar order parameter, which is given by

$$D_t \vec{P} = \frac{\vec{h}}{\gamma} - \nu \left( [\nabla \vec{v}_a]^S - \nabla \cdot \vec{v}_a \mathbb{I} \right) \cdot \vec{P} - \bar{\nu} \text{Tr}\{\nabla \vec{v}_a\} \vec{P}, \quad (7)$$

where  $\gamma$  controls the relaxation of  $\vec{P}$ , and  $D_t \vec{P} = \partial_t \vec{P} + \vec{v}_a \cdot \nabla \vec{P} + [\nabla \vec{v}_a]^A \cdot \vec{P}$ , is the objective rate (SM Sec. 4 [26]).

Activity enters explicitly into our presentation in several places. The ratio  $k$ , which governs the binding kinetics of myosin II minifilaments is active, and so is isotropic contractile term  $\zeta$ . There is also an implicit activity associated with the monopolar-like processive force  $\vec{P}$

The source/sink terms in the myosin II equation correspond to a constant myosin II minifilament on-rate and a density-dependent off-rate, with  $k$  the ‘bare’ ratio of these two quantities under  $\rho_m \rightarrow 0$ . These two expressions are coupled by force balance equations at the myosin-actin and actin-bilayer interfaces. In our layered system (Fig. 1a) these are given by:

$$\vec{v}_m = \vec{v}_a - \vec{P} - \frac{\chi_m}{\rho_m} \nabla \rho_m, \quad (3)$$

and

$$\vec{v}_a = \frac{1}{\rho_a} \nabla \cdot \Sigma - \frac{\chi_m}{\rho_a} \nabla \rho_m, \quad (4)$$

respectively. Here,  $\chi_m$  is a dimensionless isothermal compressibility for myosin II minifilaments,  $\vec{P}$  is a polar order parameter, and the tensor  $\Sigma$  is given by

in (3) (recall that the model is nondimensionalised by this characteristic myosin velocity). In principle, each of these quantities can depend on the dynamical degrees-of-freedom,  $\rho_m$ ,  $\rho_a$ , and  $\vec{P}$ . They can also depend on the concentration of available ATP, as can the dissipative coefficients of the theory.

#### IV. SCALING OF ACTIVE AND PASSIVE COEFFICIENTS

To motivate how both active and passive coefficients scale with the concentration of ATP, we examine a simple model that aims to capture the statistics of the bound status of the  $N \approx 50$  individual head groups that belong to a single minifilament.

Here, the canonical five-step ATP cross-bridge cycle [16] is approximated by a simple two-step process where headgroups bind to actin with a constant rate  $k_{\text{on}}$ , and unbind with a rate  $k_{\text{off}} \propto [\text{ATP}]$  (Fig. 2a-b). Headgroups are moreover assumed to act independently, neglecting any potential load dependence [51] and/or mechanical cooperativity [52, 53]. When  $n$  headgroups are bound, therefore, the rate of an additional binding is simply  $(N - n)k_{\text{on}}$ , whilst the rate of unbinding is  $n k_{\text{off}}$ . This results in a ladder-like stochastic process of headgroup binding and unbinding that inevitably ends with myosin II minifilament dissociation (*i.e.*, no headgroups bound). Notably, the Master equation associated with the above process can be solved recursively to yield the mean first passage time to myosin II minifilament dissociation,  $\langle T_0 \rangle$ , having started with only one bound headgroup (SM Sec. 3 [26]). This demonstrates that higher

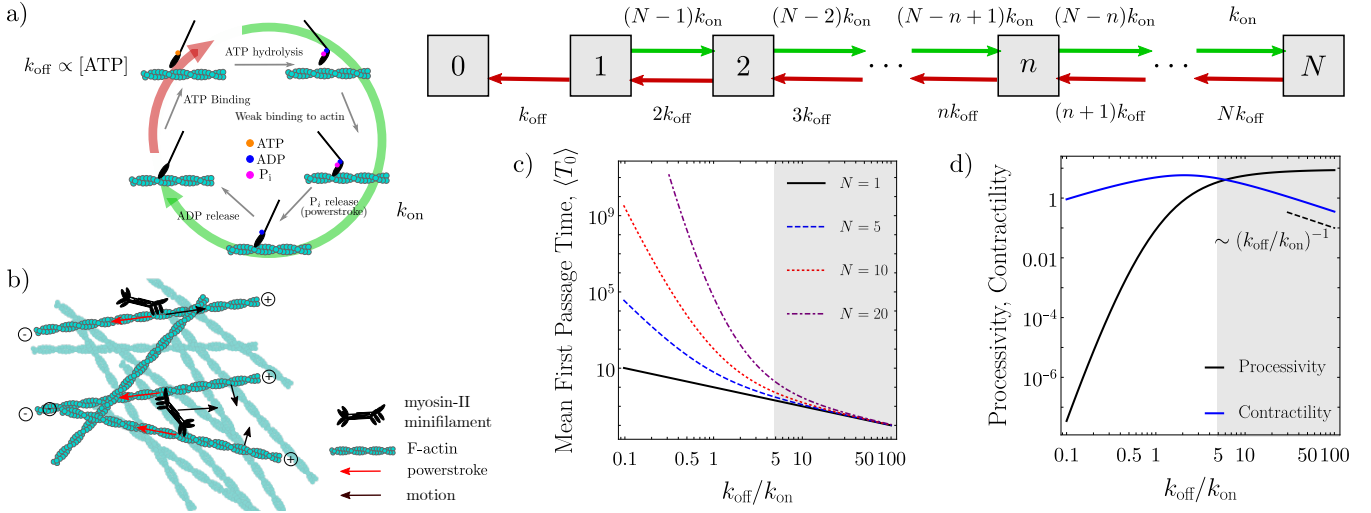


**FIG. 2. Myosin II minifilament kinetics.** **a)** Approximating the canonical 5-step ATP-cycle by a 2-step binding/unbinding process, the statistics of the bound status of a single myosin II minifilament’s head-groups can be modelled using a ladder-like state space. **b)** The power-stroke associated with the transition between singly- and doubly-bound head-groups leads to processive ‘steps’ along actin filaments, additional bound head-groups leads to crosslinking and therefore meshwork remodelling that is contractile at the hydrodynamic scale (see [46–50]). **c)** As  $k_{\text{off}} \propto [\text{ATP}]$  increases, the MFPT until myosin II minifilament dissociation converges to  $\sim 1/k_{\text{off}}$ , irrespective of the total number of head-groups, permitting us to make the identification  $k \sim \langle T_0 \rangle^{-1}$ . **d)** The rate of processive (*i.e.*,  $1 \rightarrow 2$ ) and contractile (*i.e.*,  $n \rightarrow n+1$  for  $n \neq 1$ ) power-strokes scale as a constant and  $\sim 1/k_{\text{off}}$ , respectively, as  $k_{\text{off}} \propto [\text{ATP}]$  increases.

concentrations of ATP increase the ratio of off- to on-rates and therefore decrease myosin II minifilament residence times, which is qualitatively in line with more complex models of myosin II minifilaments in the limit of low load [54, 55] and experimental observations of the duty ratio of myosin I proteins [56]. Specifically, for all appreciable levels of ATP,  $\langle T_0 \rangle \sim k_{\text{on}}/k_{\text{off}}$ , irrespective of  $N$  (Fig. 2c). Identifying the quantity  $k$  from our hydrodynamic model with  $\langle T_0 \rangle$  then implies that  $k \sim k_{\text{on}}/k_{\text{off}}$ , which not only puts macroscopic and microscopic models in contact, but also implies that  $k$  is inversely proportional to  $[\text{ATP}]$ . This is important since we expect that, in the low myosin II minifilament density regime, dissipative coefficients such as  $\eta$ ,  $\bar{\eta}$ ,  $\nu$ ,  $\bar{\nu}$ , and  $1/\gamma$  are order  $O(\epsilon)$ , where  $\epsilon = k \rho_m / \rho_a$ .

The scaling of active coefficients, by contrast, requires an argument that is based on the distribution over the *number* of state transitions—*i.e.*, the likelihood that a given transition (*e.g.*,  $n \rightarrow n+1$ ) will occur a certain number of times. The reason is that each ascending transition in our model involves a single power-stroke, and therefore the mean number of such transitions divided by the total minifilament residence time can be used as a proxy for work done. Calculating such probabilities, however, requires a sum-over-paths representation of our model. The key point being that the properties of the Laplace transform imply that the generating function of the aforementioned distribution is given by a Neumann series, and can therefore be calculated via a simple matrix inversion (SM Sec. 3 [26]).

In particular, we make a distinction between transi-

tions of the type  $1 \rightarrow 2$ , which are tantamount to taking a single processive step along the minifilament (towards the ‘plus’ end), and all other ascending transitions,  $n \rightarrow n+1$  for  $n \neq 1$ , which involve one or more bound headgroups in addition to that which performs the power-stroke. If these additional bound headgroups anchor the myosin II to either the same actin filament or another actin filament that cannot move due to meshwork frustration, then motion stalls. Otherwise, the ATP-induced power-stroke can generate relative motion between two or more actin filaments. At the scale of bulk hydrodynamic descriptions, this latter case manifests as predominantly contractile forces, since the response of actin filaments is asymmetric when subjected to either compressive or tensile loads [46–49], and the dwell time of myosin II headgroups at the plus-end of actin filaments is abnormally long [50].

Calculating the aforementioned proxies for the power associated with these two cases—‘processivity’ and ‘contractility’—implies that, as ATP increases, the former rapidly converges to a constant, whilst the latter scales like  $k$  (Fig. 2d). In the context of the hydrodynamic model, this leads us to make two assumptions. First, that  $\zeta$  has a saturating form

$$\zeta = \xi \frac{k \rho_m}{k \rho_m + \rho_a}, \quad (8)$$

for which, at low ratios of myosin II minifilaments to actin, the active contractile stress is linear in  $\epsilon = k \rho_m / \rho_a$ . Second, that the mono-polar-like processive force  $\vec{P}$  in (3) is of constant magnitude.

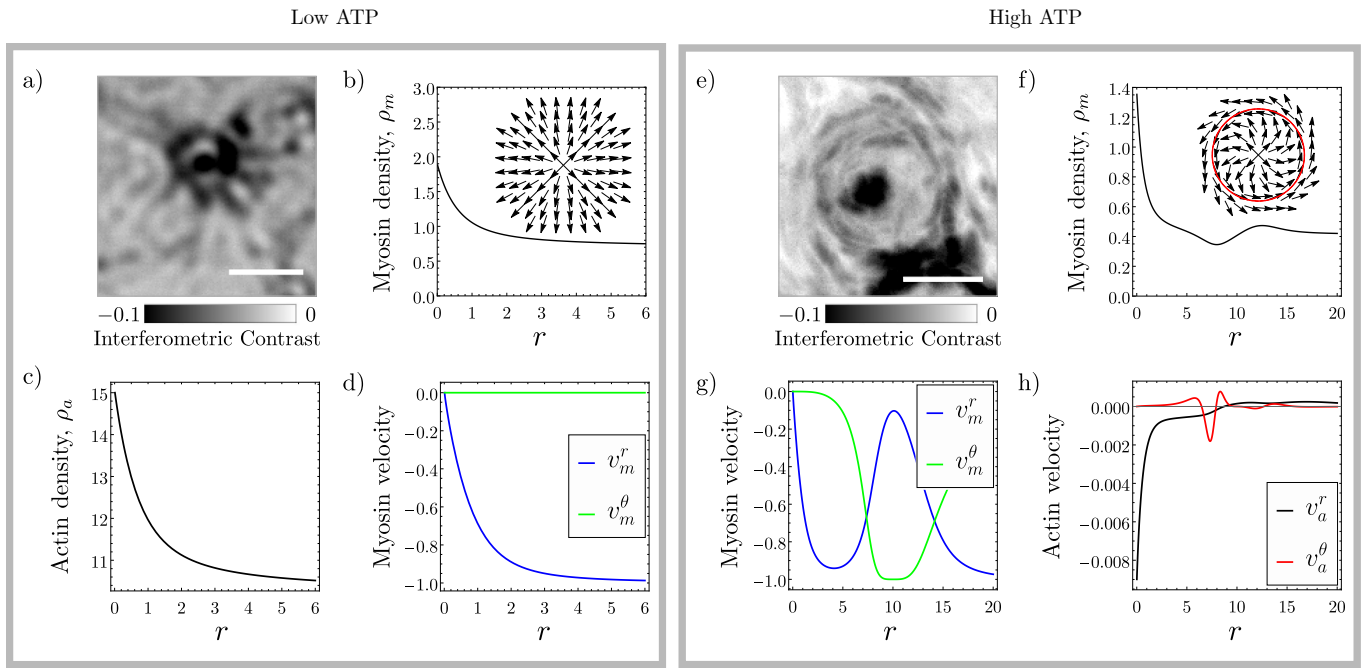


**FIG. 3. Comparing theory and experiment.** **a)** Static iSCAT microscopy image of an aster formed after depletion of ATP (20 min after addition of 0.1 mM ATP, where dark areas indicate high myosin II minifilament density (scale bar 2  $\mu$ m). On add-back of ATP, myosin II minifilaments process towards the focus of the aster (see Vid. 9 and SM Sec. 2). This compares favourably with radial steady-state solutions for **b**) myosin density, **c**) actin density, and **d**) the myosin velocity (texture shown in **b** inset). **e)** Minimal intensity projection (over 120s) of a spiral-like structure captured using iSCAT (scale bar 2  $\mu$ m) 10-15 min after addition of 0.1 mM ATP. Similarly, this compares well with radial **f**) myosin density and **g**) velocity profiles at zeroth order in  $\epsilon$  (texture shown in **f** inset). **h)** Radial actin velocity profile at  $O(\epsilon)$ . Panels **b-d** plotted for  $\xi = -1$ ,  $\chi_m = 1$ ,  $\chi_a = 0.01k$ ,  $k = 1$ . Panels **f-h** plotted for  $\xi = -1$ ,  $\chi_m = 1$ ,  $\chi_a = 0.01k$ ,  $k = 0.5$ ,  $a = 15$  and  $R = 10$ .

## V. COMPARISON BETWEEN THEORY AND EXPERIMENT

The role of the microscopically motivated scalings is to explore differences between emergent behaviours at intermediate and low ATP concentrations, and compare them with our observations.

At low levels of ATP,  $\epsilon$  is large, and therefore dissipative coefficients, active contractility and active processivity cannot be disentangled. In this case, an axisymmetric steady-state solution to Eqs. (2) and (7) is just a radial aster-like actin texture that is stationary (*i.e.*,  $\vec{P} = \vec{e}_r$  and  $\vec{v}_a = \vec{0}$ ). This implies that  $\vec{v}_m$  is a function of  $\rho_m$ , such that the accumulation of myosin II minifilaments due to their procession towards the texture's centre is balanced by the density dependent dissociation rate (see Vid. 9 and SM Sec. 2 for this behaviour in experiment). Solving this boundary value problem for  $\rho_m$  requires a shooting method. The solution can nevertheless be substituted into the remaining force balance condition, which equates contractile forces with those resisting the compression of actin. This gives a first order equation for  $\rho_a$  that is readily solvable numerically (SM Sec. 4 [26]). The resulting aster-like steady-state is depicted in Fig. 3b-d. Since it is qualitatively independent of  $k$ , we expect that the system converges to this state as ATP

depletes.

By contrast, at intermediate ATP,  $\epsilon$  is small, and we must take a perturbative approach: expanding in small  $\epsilon$  and solving hierarchically.

At zeroth order,  $\vec{v}_a^{(0)} = 0$ , implying freedom to impose  $\vec{P}^{(0)}$  and  $\rho_a^{(0)}$ . To mimic experimental motifs, we choose a spiral texture

$$\vec{P}^{(0)} = \frac{r(R^2 - r^2)^2 \vec{e}_r + \frac{a^3 r^5}{(r+R)^3} \vec{e}_\theta}{\sqrt{\left(\frac{a^3 r^5}{(r+R)^3}\right)^2 + r^2 (R^2 - r^2)^4}}, \quad (9)$$

with density profile  $\rho_a^{(0)} = cr^2 e^{-r^2/w} + l$  (SM Sec. 4 [26]). In this case, the myosin II minifilament velocity profile,  $\vec{v}_m$ , is that which balances propulsive forces with density gradients. Substituting into (1), the resulting boundary value problem is again solvable via a shooting method (SM Sec. 4 [26]). The results are in-line with experimental observations, with an inward flux of myosin II minifilaments giving way to a circular motion around a central foci, at which point the high densities are balanced by high dissociation rates.

As might be expected, this state is unstable at first order in  $\epsilon$ . We can, nevertheless, calculate first order corrections to the actin velocity profile,  $\vec{v}_a^{(1)}$ . In addition to radial corrections, this results in a small circular flow in

the same direction as the myosin II minifilaments (a phenomenon also seen in experiments, Fig. 1e & SM Sec. 2 [26]) that is accompanied by a slight shear-banding. The former is consistent with our observations, whilst the latter is either not present, or cannot be observed at the present resolution.

## VI. DISCUSSION

When taken together, experiments, single myosin II minifilament kinetics, and bulk hydrodynamics are all consistent with the notion that an increase in ATP not only increases the power of actomyosin, but it also changes the mode by which work is done. Specifically, we argue that contractile forces give way to more processivity of myosin II minifilaments at higher levels of available ATP. In other words, the concentration of ATP interpolates between active forces that are Galilean invariant and those that are not. At a hydrodynamic level, this results in a model of actomyosin that has predominantly ‘wet’ characteristics at low ATP, and ‘dry’ characteristics at intermediate ATP [17].

We speculate that this may be important for the generic understanding of actomyosin regulation. That is, in addition to phosphorylation as the canonical regulator of myosin II, ATP concentration may also be important, suggesting a link between essential functions such as contraction or shape change and the metabolic pathways by which ATP is synthesized. Such ideas may even prove relevant to understand the ramifications of a compromised metabolism [57, 58].

Nevertheless, much work needs to be done to understand how our findings translate *in vivo*, where additional complexities may include the effects of:  $\text{Ca}^{2+}$  signalling, troponin and tropomyosin [59, 60]; the effects of the small GTPase RhoA and its downstream effectors [14, 61], and; differences between branched- and linear actin [14] amongst other things.

Even in the case of our *in vitro* system there remain several aspects of our theory that might be improved upon. For the microscopic modelling, we have overlooked potential effects of load-dependence [51, 54], cooperativity [52, 53] and chirality [62], amongst others. From a hydrodynamic perspective, the chief issue is that liquid crystal-like nematic-hydrodynamic descriptions are insufficient to fully describe the remodelling of transient networks of intermediate-to-long actin filaments, which are semi-flexible and curved on length-scales similar to the filaments themselves. Whilst such networks have been

explored extensively in numerical simulations—particularly in terms of rigidification transitions and contractility generation [19, 46, 63–71]—writing down a constitutive relation for such materials is a significant outstanding challenge in the field. To our knowledge, it has only been attempted at the level of bulk passive rheology thus far, and has no straightforward generalisation to active systems [72–74]. Amongst other things, such a constitutive relation would likely need to account for the known shear-stiffening of actomyosin under imposed strain [46]. The Poisson bracket approach for computing reactive couplings in generalised hydrodynamics might prove useful here, as in nematic polymer theory [41, 75].

Regarding our experimental observations, we remark that whilst the formation of vortices and spirals have been noted in microtubule-based systems [76], similar works on actomyosin networks did not report such structures [19, 21, 28, 48, 49, 69]. This indicates that the remarkably persistent vortex- and spiral-like structures that we observe may strongly depend on the experimental conditions, including: a low actin filament concentration (equivalent to  $[\text{G-actin}] = 125 \text{ nM}$  compared to  $[\text{G-actin}] > 1 \mu\text{M}$  in other works) which lead to very thin f-actin layers ( $< 6$  filaments) [22]; the absence of crowding factors; the minimisation of laser induced photo-damage by using label-free imaging, and; degassed buffers in combination with an oxygen scavenger system, which decrease the generation of dead heads in myosin II minifilaments that would lead to irreversible crosslinking [69].

In conclusion, whilst we believe that our work highlights an important conceptual advance—ATP as a regulator as well as a fuel—there is still much work to be done. Developing more precise experimental setups (*e.g.*, microfluidic control and maintenance of ATP concentrations), more realistic microscopic theories to feed into coarse-grained hydrodynamic parameters, and better constitutive relations that capture the rheology of transient cross-linked networks are just three of the possible future directions one could take. We therefore welcome further work in this area.

## ACKNOWLEDGMENTS

RGM and SCA-I acknowledge funding from the EMBL-Australia program. DVK thanks Phillip Kukura and Nicolas Hundt for enabling the iSCAT experiments, Mohan Balasubramanian for access to the TIRF microscope, and the Wellcome-Warwick Quantitative Biomedicine Programme for funding (Wellcome Trust ISSF, RMRCB0058).

---

[1] A. Doostmohammadi, S. P. Thampi, and J. M. Yeomans, *Physical Review Letters* **117**, 048102 (2016).

[2] K. Copenhagen, R. Alert, N. S. Wingreen, and J. W. Shaevitz, *Nature Physics* **17**, 211 (2021).

[3] Q. Zhang, J. Li, J. Nijjer, H. Lu, M. Kothari, R. Alert, T. Cohen, and J. Yan, *Proceedings of the National Academy of Sciences* **118**, e2107107118 (2021).

[4] C. Blanch-Mercader, P. Guillamat, A. Roux, and

K. Kruse, Physical Review E **103**, 012405 (2021).

[5] C. Blanch-Mercader, P. Guillamat, A. Roux, and K. Kruse, Physical Review Letters **126**, 028101 (2021).

[6] R. Mueller, J. M. Yeomans, and A. Doostmohammadi, Physical Review Letters **122**, 048004 (2019).

[7] T. B. Saw, A. Doostmohammadi, V. Nier, L. Kocgozlu, S. Thampi, Y. Toyama, P. Marcq, C. T. Lim, J. M. Yeomans, and B. Ladoux, Nature **544**, 212 (2017).

[8] Y. Maroudas-Sacks, L. Garion, L. Shani-Zerbib, A. Livshits, E. Braun, and K. Keren, Nature Physics **17**, 251 (2021).

[9] S. Dasgupta, K. Gupta, Y. Zhang, V. Viasnoff, and J. Prost, Proceedings of the National Academy of Sciences **115**, E4751 (2018).

[10] R. G. Morris and M. Rao, Physical Review E **100**, 022413 (2019).

[11] G. Beaune, C. Blanch-Mercader, S. Douezan, J. Dumond, D. Gonzalez-Rodriguez, D. Cuvelier, T. Ondarçuhu, P. Sens, S. Dufour, M. P. Murrell, and F. Brochard-Wyart, Proceedings of the National Academy of Sciences **115**, 12926 (2018).

[12] H. Turlier, B. Audoly, J. Prost, and J.-F. Joanny, Biophysical Journal **106**, 114 (2014).

[13] Y. Sumino, K. H. Nagai, Y. Shitaka, D. Tanaka, K. Yoshikawa, H. Chaté, and K. Oiwa, Nature **483**, 448 (2012).

[14] S. Banerjee, M. L. Gardel, and U. S. Schwarz, Annual Review of Condensed Matter Physics **11**, 421 (2020).

[15] J. Prost, F. Jülicher, and J.-F. Joanny, Nature Physics **11**, 111 (2015).

[16] B. Alberts, A. Johnson, J. Lewis, M. Raff, K. Roberts, and P. Walter, *Molecular Biology of the Cell*, 4th ed. (Garland Science, 2002).

[17] M. C. Marchetti, J. F. Joanny, S. Ramaswamy, T. B. Liverpool, J. Prost, M. Rao, and R. A. Simha, Reviews of Modern Physics **85**, 1143 (2013).

[18] M. J. Tyska and D. M. Warshaw, Cell Motility and the Cytoskeleton **51**, 1 (2002).

[19] D. Smith, F. Ziebert, D. Humphrey, C. Duggan, M. Steinbeck, W. Zimmermann, and J. Käs, Biophysical Journal **93**, 4445 (2007).

[20] D. Mizuno, C. Tardin, C. F. Schmidt, and F. C. MacKintosh, Science **315**, 370 (2007).

[21] S. K. Vogel, Z. Petrasek, F. Heinemann, and P. Schwille, eLife **2**, e00116 (2013).

[22] L. S. Mosby, N. Hundt, G. Young, A. Fineberg, M. Polin, S. Mayor, P. Kukura, and D. V. Köster, Biophysical Journal **118**, 1946 (2020).

[23] J. Ortega-Arroyo and P. Kukura, Physical Chemistry Chemical Physics **14**, 15625 (2012).

[24] D. Cole, G. Young, A. Weigel, A. Sebesta, and P. Kukura, ACS Photonics **4**, 211 (2017).

[25] E. Meijering, M. Jacob, J.-C. F. Sarria, P. Steiner, H. Hirling, and M. Unser, Cytometry A **58**, 167 (2004).

[26] “Electronic supplementary material can be found at: ..... detailing additional figures, experimental details & calculations.”.

[27] T. Sanchez, D. T. N. Chen, S. J. DeCamp, M. Heymann, and Z. Dogic, Nature **491**, 431 (2012).

[28] D. V. Köster, K. Husain, E. Iljazi, A. Bhat, P. Bieling, R. D. Mullins, M. Rao, and S. Mayor, Proceedings of the National Academy of Sciences **113**, E1645 (2016).

[29] D. V. Köster and S. Mayor, Current Opinion in Cell Biology **38**, 81 (2016).

[30] M. Fritzsche, R. A. Fernandes, V. T. Chang, H. Colin-York, M. P. Clausen, J. H. Felce, S. Galiani, C. Erlenkämper, A. M. Santos, J. M. Heddleston, I. Pedroza-Pacheco, D. Waithe, J. B. de la Serna, B. C. Lagerholm, T.-l. Liu, T.-L. Chew, E. Betzig, S. J. Davis, and C. Eggeling, Science Advances **3**, e1603032 (2017).

[31] J. Spudich and S. Watts, J. Biol. Chem. **246**, 4866 (1971).

[32] T. D. Pollard, in *Methods in Cell Biology*, The Cytoskeleton Part A: Cytoskeletal Proteins, Isolation and Characterization, Vol. 24, edited by L. Wilson (Academic Press, 1982) pp. 333–371.

[33] W. Thielicke, *The Flapping Flight of Birds - Analysis and Application*, Ph.D. thesis, Rijksuniversiteit Groningen (2014).

[34] W. Thielicke and E. Stamhuis, Journal of Open Research Software **2**, e30 (2014).

[35] D. Garcia, Experiments in fluids **50**, 1247 (2011).

[36] Y. Tanaka, A. Ishijima, and S. Ishiwata, Biochimica et Biophysica Acta (BBA) - Protein Structure and Molecular Enzymology **1159**, 94 (1992).

[37] T. Nishizaka, T. Yagi, Y. Tanaka, and S. Ishiwata, Nature **361**, 269 (1993).

[38] E. M. De La Cruz, J. Roland, B. R. McCullough, L. Blanchoin, and J.-L. Martiel, Biophysical Journal **99**, 1852 (2010).

[39] K. Kruse, J. F. Joanny, F. Jülicher, J. Prost, and K. Sekimoto, Physical Review Letters **92**, 078101 (2004).

[40] A. Das, A. Bhat, R. Sknepnek, D. Köster, S. Mayor, and M. Rao, Science Advances **6**, eaay6093 (2020).

[41] P. Chaikin and T. Lubensky, *Principles of Condensed Matter Physics* (Cambridge University Press, 2000).

[42] K. Kruse, J. F. Joanny, F. Jülicher, J. Prost, and K. Sekimoto, The European Physical Journal E **16**, 5 (2005).

[43] K. Husain and M. Rao, Physical Review Letters **118**, 078104 (2017).

[44] K. Gowrishankar and M. Rao, Soft Matter **12**, 2040 (2016).

[45] P. de Gennes and J. Prost, *The Physics of Liquid Crystals*, International Series of Monogr (Clarendon Press, 1993).

[46] G. H. Koenderink, Z. Dogic, F. Nakamura, P. M. Bendix, F. C. MacKintosh, J. H. Hartwig, T. P. Stossel, and D. A. Weitz, Proceedings of the National Academy of Sciences **106**, 15192 (2009).

[47] I. Linsmeier, S. Banerjee, P. W. Oakes, W. Jung, T. Kim, and M. P. Murrell, Nature Communications **7**, 12615 (2016).

[48] M. P. Murrell and M. L. Gardel, Proceedings of the National Academy of Sciences **109**, 20820 (2012).

[49] Y. Ideses, A. Sonn-Segev, Y. Roichman, and A. Bernheim-Groswasser, Soft Matter **9**, 7127 (2013).

[50] V. Wollrab, J. M. Belmonte, L. Baldauf, M. Leptin, F. Nédeléc, and G. H. Koenderink, Journal of Cell Science **132**, jcs219717 (2019).

[51] E. P. Debold, J. B. Patlak, and D. M. Warshaw, Biophysical Journal **89**, L34 (2005).

[52] S. Walcott, D. Warshaw, and E. Debold, Biophysical Journal **103**, 501 (2012).

[53] M. Kaya, Y. Tani, T. Washio, T. Hisada, and H. Higuchi, Nature Communications **8**, 16036 (2017).

[54] T. Erdmann, K. Bartelheimer, and U. S. Schwarz, Physical Review E **94**, 052403 (2016).

[55] P. J. Albert, T. Erdmann, and U. S. Schwarz, New Journal of Physics **16**, 093019 (2014).

[56] C. Veigel, L. M. Coluccio, J. D. Jontes, J. C. Sparrow, R. A. Milligan, and J. E. Molloy, *Nature* **398**, 530 (1999).

[57] M. A. Jansen, H. Shen, L. Zhang, P. E. Wolkowicz, and J. A. Balschi, *American Journal of Physiology-Heart and Circulatory Physiology* **285**, H2437 (2003).

[58] N. Smith and E. Crampin, *Progress in Biophysics and Molecular Biology* **85**, 387 (2004).

[59] P. VanBuren, K. A. Palmiter, and D. M. Warshaw, *Proceedings of the National Academy of Sciences* **96**, 12488 (1999).

[60] N. M. Kad, S. Kim, D. M. Warshaw, P. VanBuren, and J. E. Baker, *Proceedings of the National Academy of Sciences* **102**, 16990 (2005).

[61] S. Budnar, K. B. Husain, G. A. Gomez, M. Naghibosadat, A. Varma, S. Verma, N. A. Hamilton, R. G. Morris, and A. S. Yap, *Developmental Cell* **49**, 894 (2019).

[62] Y. H. Tee, T. Shemesh, V. Thiagarajan, R. F. Hariadi, K. L. Anderson, C. Page, N. Volkmann, D. Hanein, S. Sivaramakrishnan, M. M. Kozlov, and A. D. Bershadsky, *Nature Cell Biology* **17**, 445 (2015).

[63] D. A. Head, A. J. Levine, and F. C. MacKintosh, *Physical Review E* **68**, 061907 (2003).

[64] D. A. Head, A. J. Levine, and F. C. MacKintosh, *Physical Review Letters* **91**, 108102 (2003).

[65] K. Kasza, C. Broedersz, G. Koenderink, Y. Lin, W. Messner, E. Millman, F. Nakamura, T. Stossel, F. MacKintosh, and D. Weitz, *Biophysical Journal* **99**, 1091 (2010).

[66] B. Stuhrmann, M. Soares e Silva, M. Depken, F. C. MacKintosh, and G. H. Koenderink, *Physical Review E* **86**, 020901 (2012).

[67] T. H. Tan, M. Malik-Garbi, E. Abu-Shah, J. Li, A. Sharma, F. C. MacKintosh, K. Keren, C. F. Schmidt, and N. Fakhri, *Science Advances* **4**, eaar2847 (2018).

[68] Y. Mulla, F. MacKintosh, and G. H. Koenderink, *Physical Review Letters* **122**, 218102 (2019).

[69] J. Alvarado, M. Sheinman, A. Sharma, F. C. MacKintosh, and G. H. Koenderink, *Nature Physics* **9**, 591 (2013).

[70] S. Arzash, P. M. McCall, J. Feng, M. L. Gardel, and F. C. MacKintosh, *Soft Matter* **15**, 6300 (2019).

[71] F. Nédélec and D. Foethke, *New Journal of Physics* **9**, 427 (2007).

[72] F. Tanaka and S. F. Edwards, *Macromolecules* **25**, 1516 (1992).

[73] F. Tanaka and S. F. Edwards, *Journal of Non-Newtonian Fluid Mechanics* **43**, 273 (1992).

[74] F. Tanaka and S. F. Edwards, *Journal of Non-Newtonian Fluid Mechanics* **43**, 247 (1992).

[75] R. Kamien, *Physical Review E* **61**, 2888 (2000).

[76] F. J. Nédélec, T. Surrey, A. C. Maggs, and S. Leibler, *Nature* **389**, 305 (1997).